Design and experimental investigation of a vibro-impact capsule robot for colonoscopy*

Jiajia Zhang[1], Yang Liu[1], Jiyuan Tian[1], Dibin Zhu[2] and Shyam Prasad[3]

Abstract— **Uptake of capsule endoscopy in the large intestine has been very limited due to both the risk of missed lesions and the often prolonged transit time, making it an unviable alternative to standard colonoscopy. In this letter, we presented a controllable and easy-to-use diagnostic tool, equipping a novel vibration module inside a capsule robot for colonoscopy. The capsule's motion was controlled by applying an external alternating electromagnetic field to the capsule's inner magnet to generate vibrations and impacts on the main body of the capsule. To optimise its motion, we provided a numerical solution for calculating its electromagnetic force and used it to guide a hand-held control panel for navigating the robot. The robot was firstly examined in a large intestine simulator modelled based on the colon-rectal morphometrics, and then tested in an *ex vivo* environment using porcine intestines. We verified the performance of the robot travelling through the entire intestine with the maximum speeds of 54 mm/s and 40 mm/s in the simulator and the *ex vivo* environment, respectively. It was found that altering the control frequency of the panel can help the robot to pass through various morphometrics, in particular the sharp turnings at the segment junctions.**

I. INTRODUCTION

Early diagnosis of bowel cancer can highly increase survival rate, while early detection crucially requires regular check-up of the large intestine [1]. In a retrospective analysis [2], patients with potential bowel cancer are in high command of going through check-up with short intervals. Such a high demand will be an overwhelming burden to the medical system, including increasing learning curves for operators and caring people, taking hygienic procedure of the flexible colonoscopy, and also causing discomfort and critical complications to the patients. During and after the pandemic of Covid-19, large intestine examinations have been greatly reduced, resulting in more waiting times for colonoscopies [3]. A wider coverage of adoption in disposal and remotely-controllable diagnostic tools could be highly beneficial to fulfil this gap. Therefore in colonoscopic practice, there is an urgent need for new modalities that are safe, painless and reliable, which require minimal training for practitioners.

Developing soft-tethered or untethered capsules for colonoscopy has been of great interests by robotics researchers for the past two decades. One diagnosis study carried out by passive capsule endoscope on 2485 patients concluded that it reached an effective detection rate of 93% and no complications were reported [4]. But for such a passive capsule endoscope, drawbacks are: (i) the capsule is swallowed from the mouth and travels for 8-10 hours to reach the rectum, and by reaching the cecum, the miniaturised camera on the capsule is usually not clean enough with a poor vision for diagnosis; (ii) passive capsule is not controllable inside the large intestine; (iii) in a large-scale capsule retention study [5], it was found that the capsule retention rate was 0.75%-2.5%. Thus, capsule engineers were keen to inject new ideas to overcome these limitations, and new controllable capsules with better reliability were extensively developed in the past two decades.

Among all the solutions which include but not limit to the design of capsule colonoscopes, Poon et al. [6] designed a caterpillar-like locomotive module; Lee et al. [7] designed a reel-mechanism based robotic colonoscope. Pneumatic designs are also prevalent in colonoscope designs. For example, a nature-inspired soft pneumatic origami structure was adopted into gastrointestinal endoscopic application [8]; a snail-like soft robot was proposed that can crawl on uneven surfaces [9]. Magnetic-guided actuation method was also employed, especially in capsule colonoscopy designs [10]. Systematic modelling between two permanent magnets was studied in [11]. This approach can simplify the arrangement inside the capsule and precisely control its orientation as well as induce relative motion [12]. Related research works include a simultaneous magnetic actuation and localisation endoscopy system [13], a commercial magnetic controlled stomach capsule [14], an autonomous magnet-guided flexible colonoscopy system [1], a soft capsule equipped with fine-needle being controlled magnetically [15], levitation system to reduce contact with the environment and facilitate locomotion [16], a designed magnetic system with mapped magnetic field and torque [17], and a cascaded multi-functional magnetic-controlled robot with docking separation [18]. By evaluating these studies and addressing the unsolved issues, we adopted a magnetic actuation scheme in our design to bypass intricate mechanisms and avoid excess on-board power requirements within a pill-sized capsule.

This letter demonstrates a controllable capsule robot based on the vibro-impact driving method spearheaded in [19]. The principle of the method is illustrated in Fig. 1, where the progression of the robot can be generated using a periodically

---

*This work was supported by the EPSRC under Grant No. EP/R043698/1. For the purpose of open access, the authors have applied a Creative Commons Attribution (CC BY) licence to any Author Accepted Manuscript version arising.

[1] J. Zhang, Y. Liu and J. Tian are with Engineering Department, University of Exeter, Exeter EX4 4QF, UK. `jz431,y.liu2,jt535@exeter.ac.uk`

[2] D. Zhu is with School of Electronic Information and Electrical Engineering, Shanghai Jiao Tong University, 800 Dong Chuan Road, Shanghai, 200240, China. `d.zhu@sjtu.edu.cn`

[3] S. Prasad is with Endoscopy Department, Royal Devon University Healthcare NHS Foundation Trust, Barrack Road, Exeter, EX2 5DW, UK. `shyamprasad@nhs.net`

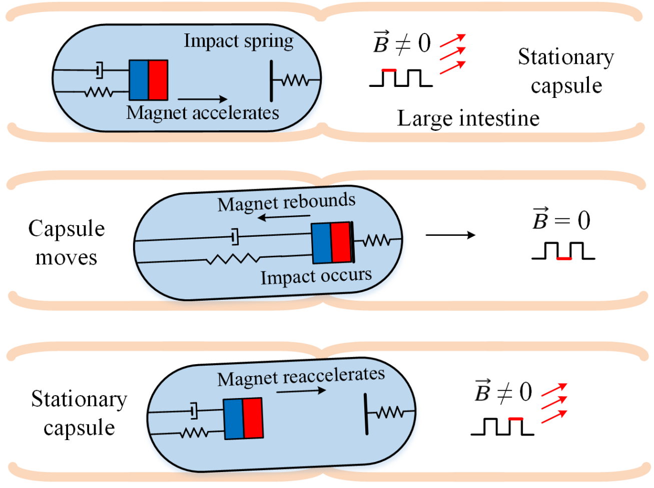

Fig. 1. Principle of the vibro-impact driving method: a permanent magnet inside a capsule was excited via an on-off electromagnetic field (square wave) leading to both horizontal and tilted movements of the robot. The robot was placed inside a customised large intestine simulator with haustral folds and can cross these folds and pass sharp turns in the simulator.

driven internal mass interacting with the main body of the robot as a "hammer", in the presence of external resistances. The entire capsule will be progressing at its maximum during the resonance of the "hammer". The dynamic behaviour of the robot will be greatly affected by its complex environmental conditions, such as in the intestinal tract [20]. A miniaturised capsule prototype adopting external magnetic actuation was studied in [21]. Earlier studies on vibrational capsule [22] revealed that vibrations could be a potential means to reduce capsule-intestine resistances.

As a successive design adopted from [21], the main contributions of this work are summarised as follows. (1) The focus of this letter is to demonstrate the effectiveness of using vibro-impact method to drive the capsule robot for colonoscopy. Thus an external electromagnet system was developed to control the robot's internal permanent magnet (IPM). (2) The external coil in this design was placed on top of the capsule, rather than in front of the capsule as studied in [21]. By doing this the coil can be flexibly placed along the patient's abdomen, either above or beneath the capsule robot; while in the previous design, the coil should be strictly placed at the concentric position of the capsule which is difficult to maneuver. (3) Since electromagnetism was adopted, the efficiency of this system was investigated through a dedicated coil shape optimisation. This will help to improve the power supply efficiency when the external electromagnetic system indeed offers a viable solution to simplify the control of an untethered robot. (4) To study the distribution of the magnetic force generated by the control coil, and to prepare a further real-time close-loop control, a numerical model for calculating the magnetic force was illustrated. This model can provide precise force information to guide the coil's movement when the position and orientation of the capsule robot are known. (5) A simulator replicating the anatomical lumen was built to provide a testing environment for the capsule robot. The robot's dynamics were found to be various at different parts of the large intestine. This observation can be used to develop a solution to alter the robot's control parameters (e.g., excitation frequency) in real time to help it travel through the large intestine efficiently.

II. METHOD

A. Design of the capsule robot

The proposed robot aims to move along the large intestine through patient's anus towards the cecum as illustrated in Fig. 2, and the design requirements are listed as below.

- The dimension of the capsule should be suitable for easy steering in the large intestine regardless of sharp turning angles and narrow-tract conditions.
- The inner magnet should be made with sufficient size to generate adequate force to propel the capsule.
- The overall weight of the robot should be as light as possible, to be capable to tilt up to climb over the haustral folds of the large intestine.
- The surface of the capsule's body should be smooth (no outer propelling mechanisms) to reduce the potential damage to the intestine. In addition, the capsule should be tightly sealed so that no infiltration of liquid will happen when travelling inside a fluid environment.

Taking these requirements into consideration, the designed robot includes the following components: a T-shaped IPM (head diameter = 15 mm and length = 9 mm, tail diameter = 12 mm and length = 15 mm) with a helical spring connecting its body with the capsule shell, which has two constraints at both ends of the magnet to exert impacts. The T-shaped IPM weighing 24.63 g in total was assembled by several permanent magnets made of Neodymium in cascade. The dimension of the capsule is 19 mm in diameter and 47.6 mm in length with a total prototype weight of 30.61 g. This size will ensure that the robot can climb haustral folds, pass sharp turns and turn around easily in the large intestine, while offering enough inner space for magnet actuation. Finally, the capsule shell was designed to be lightweight and fabricated via the fused filament fabrication 3D printing technique using polylactic acid while guaranteeing functioning properly.

B. Coil design and optimisation

Steering is essential for the capsule system to safely travel through the large intestine. Being able to steer means it can change the orientation of the camera during examination. In this case, steering is realised by hand control of an external electromagnetic coil, which can generate the excitation force in a predictable orientation on the robot. Driving the robot through the external electromagnetic coil normally has a high energy consumption, because a large electromagnetic coil will inevitably have a low working efficiency compared to the permanent magnet [1], [13] due to heat loss. To improve the efficiency, coil optimisation is necessary to get sufficient force while keeping power consumption as low as possible. In this case, according to

$$P = I^2R = I^2\rho\tfrac{l}{A}, \tag{1}$$

the power consumption of a certain coil P is determined by the total length of the wire l once the applied current to the

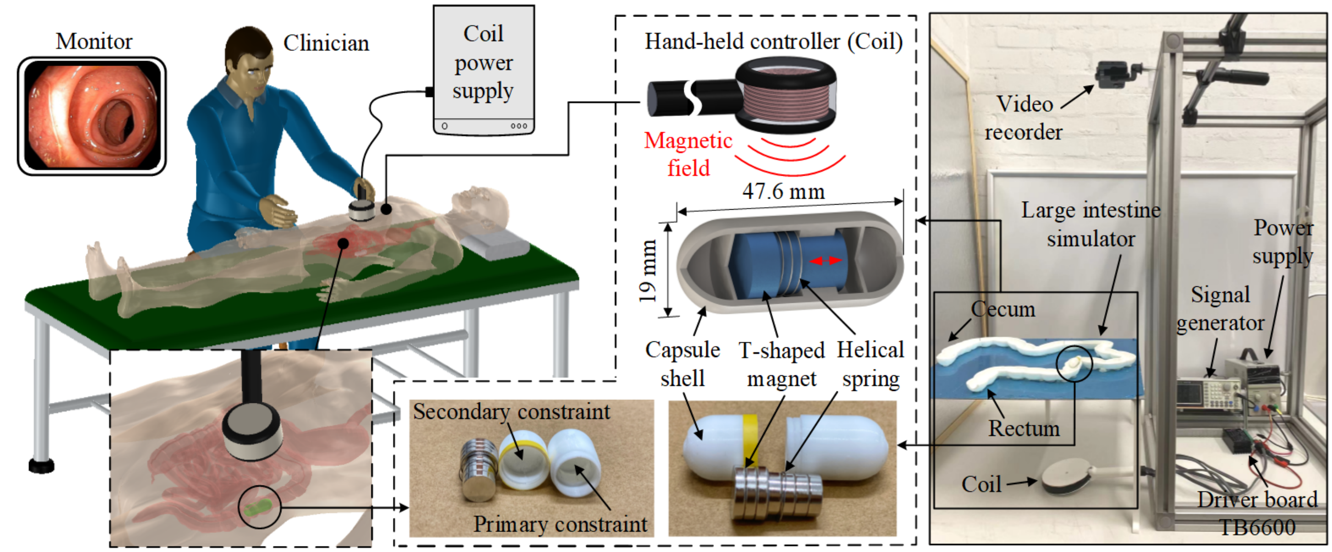

Fig. 2. Conceptual design and real-world platform of our proposed capsule system for colonoscopy, where a capsule prototype (47.6 mm in length and 19 mm in diameter) was designed for experimental testing. The prototype contains a T-shaped permanent magnet for vibration, a helical spring for reverting the magnet's position and a capsule shell with a primary and a secondary constraints for restricting the vibration of the magnet. Once the magnet is excited by the external electromagnetic field using a square wave signal, it may impact with the constraints, so the prototype can progress either forward or backward. During the colonoscopy procedure, a clinician will hold a coil panel above the capsule robot, and the robot will be excited and travel from the patient's rectum to the cecum for examination. For our experimental setup, we fabricated a simulator to mimic the environment of the intestinal tract. In our experiment, we controlled the prototype by putting the coil panel under the platform, so the video camera can record the locomotion of the robot.

coil I, resistivity of the wire ρ and cross-sectional area of the wire A are predefined. Besides the length of the wire, coil geometry can affect the magnetic force applied to the IPM, in both magnitude and direction. With an appropriate shape optimisation, we can use a shorter wire to achieve the same goal where the coil generates the desired driving force on the IPM. In the experiment, we fixed ρ, A, I and l before carrying out shape optimisation, so in theory the total power consumption of 18.13 W was also fixed, where the total resistance for the coil was 37 Ω and the applied voltage was 25.9 V. According to Fig. 3, there are three parameters to determine a coil's shape: the outer radius R, the inner radius r and the coil's thickness L. As the total length of the wire is fixed, these three parameters are related to each other and interactively affect the generated magnetic field. Our coil optimisation aims to find the best relation between these three parameters, to provide an optimum force within the control area to drive the robot.

A relationship can be built with the total volumes of the wire and the coil, considering that the coil is not fully filled by the wire but still leaves some gaps between the winding

$$l\,\pi\,\tfrac{d^2}{4} = F_\mathrm{c}\,L\,\pi\,(R^2 - r^2), \tag{2}$$

where d is the diameter of the wire, F_c is the coil fill factor that is the ratio of the volume of the wire to the volume of the coil. Thus, the thickness of the coil can be written as

$$L = \tfrac{l\,d^2}{4(R^2-r^2)F_\mathrm{c}}. \tag{3}$$

The total turns of the coil can be calculated as

$$t = \tfrac{4F_\mathrm{c}(R-r)L}{\pi d^2}. \tag{4}$$

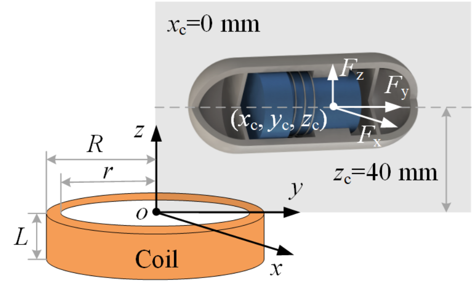

Fig. 3. Schematic of the coil setup, where R, r and L are the optimisation parameters, and the total length of the wire was fixed at l=440 m. For optimisation, the coil was fixed and the capsule (or the IPM) moved along y axis with x_c=0 mm, $y_\mathrm{c} \in [0, 100]$ mm, and z_c=40 mm. The force magnitudes generated on the IPM, F_y and F_z, will be calculated.

Simulations using ANSYS Maxwell were conducted to quantify the generated force by changing the coil's shape parameters. In the simulation, the IPM with a magnetisation magnitude 8.38×10^5 A/m and a total volume 3.29×10^{-6} m^3, was placed above the coil with an operation distance of z_c=40 mm as shown in Fig. 3. The forces applied on the magnet (F_y and F_z) along its horizontal line were recorded for $y \in [0, 100]$ mm. Here, an ideal solution is to have a series of large horizontal forces F_y that can transform into impact forces; and a series of small vertical forces F_z to control the tilted motion of the robot. Selection of coil's shape parameters was done by fixing R and r, while L and t can be calculated using Eqs. (3) and (4). In the simulation, we assumed F_c=1, and the boundaries were set with percentage offset, padding type in 150%, padding data in x, y and z directions, air filled, and the percentage error of self-convergence was set to 0.2%. Finally, a total of 17 cases as listed in Table I were simulated.

TABLE I

VARIOUS CONFIGURATIONS FOR COIL OPTIMISATION.

R (mm)	r (mm)	L (mm)	No. of turns	L_i (Henry)
30	5	31.4	3928	0.233
30	10	34.4	3437	0.236
30	15	40.7	3055	0.228
30	20	55	2750	0.200
30	25	100	2500	0.133
40	10	18.3	2750	0.242
40	20	22.9	2292	0.254
40	30	39.3	1964	0.224
50	10	11.5	2292	0.218
50	20	13.1	1964	0.237
50	30	17.2	1718	0.250
50	40	30.5	1527	0.231
60	10	7.9	1964	0.190
60	20	8.6	1718	0.207
60	30	10.2	1528	0.225
60	40	13.75	1375	0.239
60	50	25	1250	0.227

Fig. 4 presents some example results for different coil configurations, where F_{y} and F_{z} were calculated for x_{c}=0 mm, $y_{\mathrm{c}} \in$ [0, 100] mm and z_{c}=40 mm. Here, our range of interest is $y_{\mathrm{c}} \in$ [60, 100] as it can provide a large F_{y} but a small F_{z}. By analysing all the simulation results of 17 configurations, it was found that a smaller r will result in a large F_{y} but a small F_{z}, while a larger R may lead both F_{y} and F_{z} to be large. Here, a trade-off between large F_{y} and small F_{z} was made.

As the frequency applied to the coil is up to 100 Hz, a frequency response analysis will be carried out next. The inductive reactance of the coil can be written as

$$X_L = 2\pi f L_i, \tag{5}$$

where L_i is the inductance of the coil depending on the number of turns, outer diameter R, inner diameter r and the total length of the wire l according to [24]. The inductance L_i under different coil configurations was listed in Table I, where two configurations, (R, r)=$(30, 25)$ mm and (R, r)=$(60, 10)$ mm, are lower than 0.2 H. Considering all the above discussions, our optimum configuration for the coil was chosen at (R, r)=$(60, 10)$ mm.

A numerical solution is exemplified here for predicting the force generated on the IPM according to the capsule's position $(x_{\mathrm{c}}, y_{\mathrm{c}}, z_{\mathrm{c}})$, which can be written as [21]

$$\vec{P}_d = v\ (\vec{M}\cdot\nabla)\vec{B} = v\ M\ [\frac{\partial B_x}{\partial x}\quad \frac{\partial B_y}{\partial x}\quad \frac{\partial B_z}{\partial x}]^T, \tag{6}$$

where M is magnet's magnetisation value, v is magnet's volume, and B is the magnetic field solving via [25]

$$B_x = \frac{\mu_0 I}{4\pi}\int_0^L\int_r^R\int_0^{2\pi}\frac{a(b+h)\cos\theta}{\chi^{3/2}}\mathrm{d}\theta\mathrm{d}a\mathrm{d}h, \tag{7}$$

$$B_y = \frac{\mu_0 I}{4\pi}\int_0^L\int_r^R\int_0^{2\pi}\frac{a(b+h)\sin\theta}{\chi^{3/2}}\mathrm{d}\theta\mathrm{d}a\mathrm{d}h, \tag{8}$$

$$B_z = \frac{\mu_0 I}{4\pi}\int_0^L\int_r^R\int_0^{2\pi}\frac{a(a-y\sin\theta-x\cos\theta)}{\chi^{3/2}}\mathrm{d}\theta\mathrm{d}a\mathrm{d}h, \tag{9}$$

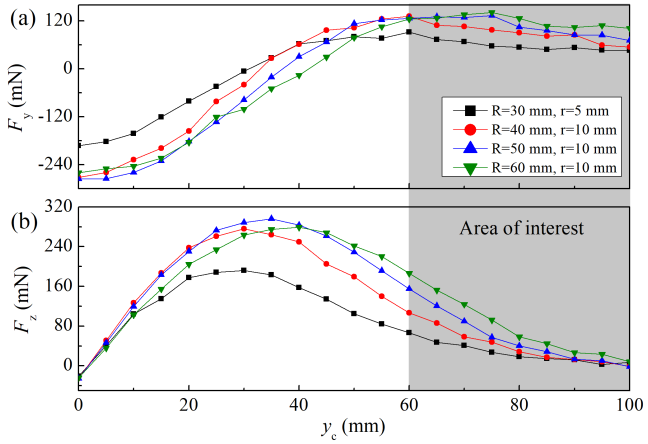

Fig. 4. Example results for different coil configurations, where (a) F_{y} and (b) F_{z} were calculated for x_{c}=0 mm, $y_{\mathrm{c}} \in$ [0, 100] mm and z_{c}=40 mm.

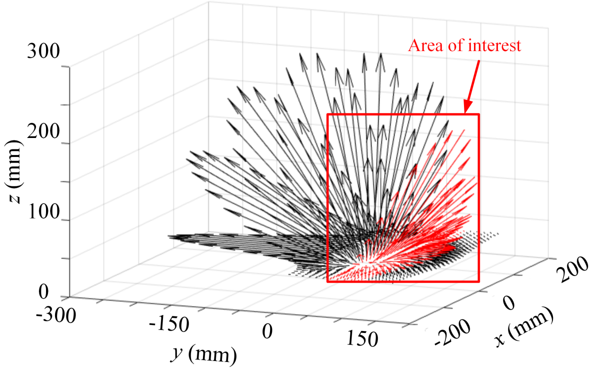

Fig. 5. (a) Force vectors on the magnet at z_{c} = 40 mm. Vectors in $y_{\mathrm{c}} \in$ [60, 100] mm marked by red colour indicate the area of interest used for driving the capsule. In this area, the forces point towards the forward-upward (positive y and z) direction.

where μ_0 is the magnetic constant, a is the radius, b is z_{c}, $b+h$ is the distance from the coil to the IPM, and $\chi = (x - a\cos\theta)^2 + (y - a\sin\theta)^2 + (b+h)^2$. Fig. 5 presents a 3D vector plot obtained using Eqs. (6)-(9) to show the magnetic fields generated by the coil and the area of interest that was used to drive the capsule.

C. Coil fabrication

After the optimisation of coil shape was finished, the coil was fabricated by the following steps: (i) The coil's body frame and handle were designed in SolidWorks and 3D-printed by the fused filament fabrication method using polylactic acid material. (ii) Wire sized in AWG 24 was wound to the coil's body frame. (iii) The handle was connected to the coil's body frame, and the input and output wires were extended through the handle, then soldered to a socket which was connected to the end of the handle. (iv) A power cable soldered with an adaptive plug at two ends was fabricated to make it safely power up the coil with a high-voltage and high-current power supply.

The parameters of the coil fabricated and used in the experiment were adopted from the optimisation results. As mentioned before, the number of turns is smaller than the

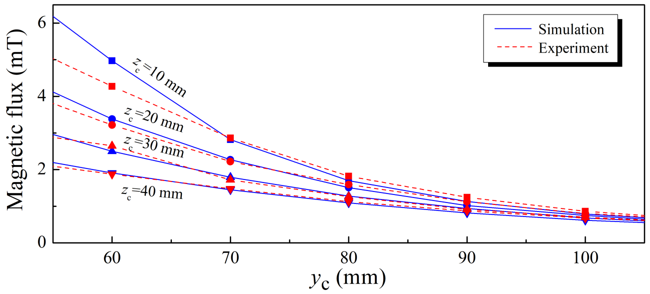

Fig. 6. Magnetic flux densities at different y_c and z_c positions generated by the optimised coil and compared with the simulation results obtained from ANSYS Maxwell. All these flux densities were tested under the maximum current capacity of the coil at 0.7 A.

ideal calculation due to the wiring containing air gaps. To validate the coil's performance, a Gauss meter (Hirst Magnetics GM07) was used to measure the magnetic flux strength generated by the coil and compared with the simulation results obtained from ANSYS Maxwell as shown in Fig. 6. Overall, the magnetic flux strength differences are obvious between the simulation and experimental results, but the difference becomes smaller in our area of interest, i.e., $y_c \in [60, 100]$ mm and z_c=40 mm.

D. Large intestine simulator model

In the experiment, the capsule robot was tested by using a human large intestine simulator designed and fabricated in our laboratory. The model was designed to simulate the morphometrics of human anatomical colon tract, including rectum, sigmoid colon, descending colon, transverse colon and ascending colon. The model was designed by using SolidWorks, printed by Flashforge Adventure 3 using the fused filament fabrication 3D printing technique and the polylactic acid materials, which followed the same fabrication process as the capsule shell and the coil panel.

According to [23], for each segment of the large intestine, there are some noticeable differences in length, diameter, fold height and number of haustral folds. The simulator shown in Fig. 7 was designed based on the data presented in [23], and its key design parameters are given in Table II, where L_s is the section length, D_{avg} is the average diameter, H_{max} is the maximum fold height, and ϕ_{max} is the maximum turning angle. The total length of the model is about 1600 mm. To better quantify the capsule's moving efficiency at specific turns, the simulator model was divided into 12 sections (turns) as shown in Fig. 7.

TABLE II

KEY DESIGN PARAMETERS OF THE SIMULATOR.

Segment	L_s (mm)	D_{avg} (mm)	H_{max} (mm)	ϕ_{max}
Rectum	234	36	5.8	17°
Sigmoid	276	30	5.9	64°
Descending	242	33	6.4	52°
Transverse	572	40	5.2	87°
Ascending	217	45	4.7	24°
Cecum	69	40	5.0	0°

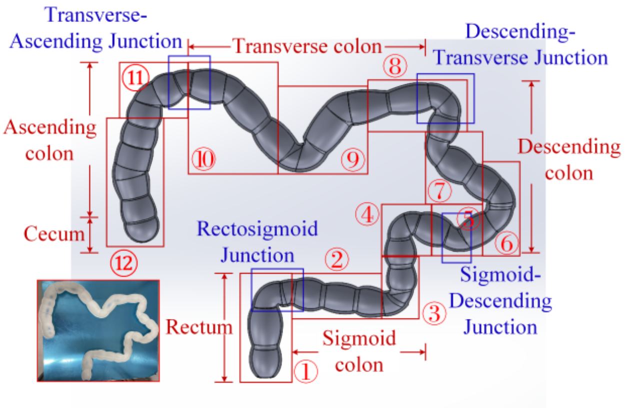

Fig. 7. Large intestine simulator assembly in SolidWorks with sections labelled by red texts and key junctions denoted in blue, and the prototype shown in left-bottom panel was divided into 12 sections for experiments.

E. Experimental procedures

As can be seen from the experimental rig shown in Fig. 2, the driving signal was generated from a signal generator and amplified by a stepper motor driver board TB6600 as a signal amplifier. The output of the signal amplifier was connected to a designed hand-held magnetic coil. During the experiment, an operator held and maneuvered the coil underneath the blue bench and control the capsule from real-time observation. There are several existing methods for the closed-loop control of capsule endoscopy (e.g., [12], [13]). However, our primary focus of this work is to demonstrate the proposed vibro-impact driving method for capsule colonoscopy. Thus, a closed-loop control system will be considered in a separate publication. To this end, the moving trajectory of the capsule was recorded by the video camera on the top of the bench, and the recorded videos were analysed to examine the behaviours and calculate the progression speeds. Each experiment was finished by a complete run starting from the rectum to the cecum.

After the videos for each experiment were collected, they were imported into Matlab for analysis. A coordinate system on bench plane was built upon the image, and the capsule's position at each frame was stored by the distance to the origin of the coordinate system. The position of the capsule was extracted by edge detection of the yellow marker attached to the capsule and Hough transform calculation. To reduce the chance of wrong edge taken and improve the video processing efficiency, the imported videos were transformed into a rate of two frames per second before processing. The extracted information contains the time used to travel to the position. Frames with wrongly-taken mark positions were checked and corrected manually.

Two experiments, namely preliminary and secondary experiments were designed and conducted inside the lower bowel simulator, and the details will be given in the next section. One time in the preliminary experiment and five repeats in the secondary experiment were conducted under each control parameter group. Human errors introduced by manual control were mitigated by practising before the experiments. After two rounds of the experiments, further

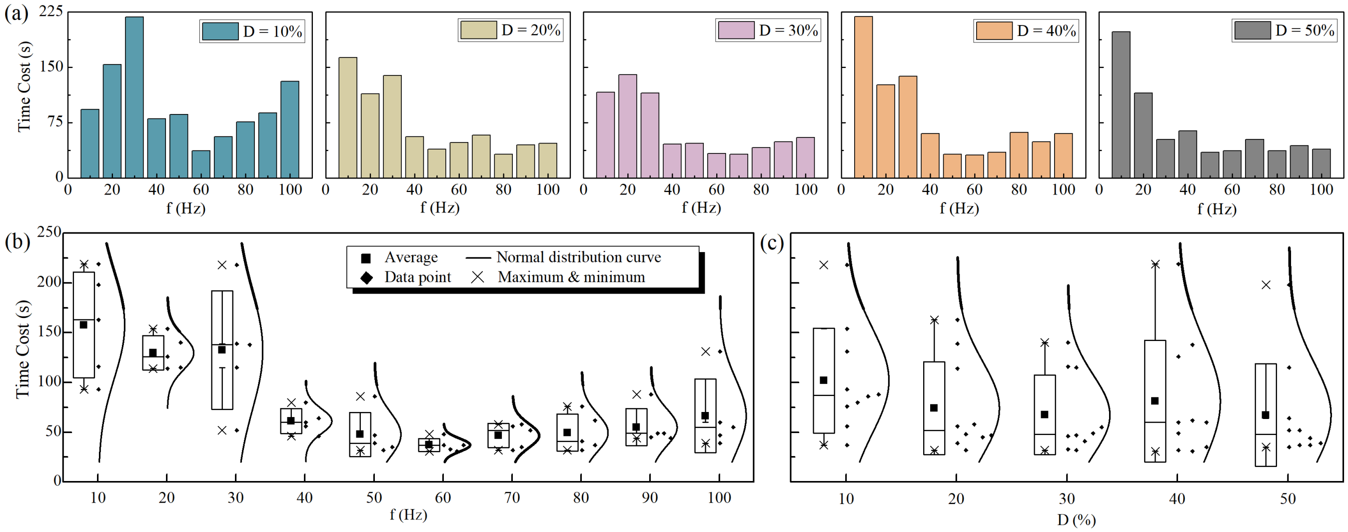

Fig. 8. (a) Preliminary experiments with the time cost (the maneuver time from the rectum to the cecum) recorded under different control frequencies $f \in [10, 100]$ Hz and duty cycles $D \in [10\%, 50\%]$. Box charts comparing between groups of different f ranging from 10 Hz to 100 Hz. The data points are from the preliminary experiments while under each frequency with five duty cycle changes in 10%, 20%, 30%, 40% and 50%. The average point, normal distribution curve, data points and the maximum and minimum points of each group are given in the comparisons of (b) f and (c) D.

tests were carried out inside the bare colon simulator with a plastic surface, and an *ex vivo* environment was prepared with porcine intestine tissue covering the surface of the simulator while the tissue was maintained in the simulator's shape. Fresh porcine intestine was cut open and placed along the simulator tract with its inner side exposed. The humidity was kept constant during the experiment to maintain a similar friction environment throughout the experiment, as well as to be closer to the real scenario. All the *ex vivo* experiments were conducted on the same day.

III. RESULTS

Our conducted experiments mainly focused on investigating the best operational ranges for the frequency f and duty cycle D of excitation force of the coil panel, to produce the most efficient progression speed. In this section, the results acquired from Matlab video analysis were classified and presented to support further discussions. Fig. 8(a) provides a summary of the preliminary experiments, where the influence of f and D was revealed. The preliminary experiments were divided into 50 parameter groups within a combination of frequency ranged in $f \in [10, 100]$ Hz with an interval of 10 Hz, and duty cycle ranged in $D \in [10\%, 50\%]$ with an interval of 10%. The preliminary frequency range was determined according to our previous studies on the dynamics of this capsule model [21]. From the preliminary experiment, it was found that the time cost is related to robot's stability, and $f \in [40,\ 80]$ Hz with D=30% is the optimum range, which was applied to the secondary experiment for stability tests, where tests were repeated to assess capsule's maneuvering robustness.

A. Preliminary frequency

To compare the time cost (the maneuver time from the rectum to the cecum) under different f, we considered D from 10% to 50% for each group of f. Data points illustrated in Fig. 8(b) indicate each experiment under certain D, where in each f there are five data points. From the experiment data, the best working f is 60 Hz, with the shortest average travelling time of 37.2 seconds and the most stable behaviour (a narrow normal distribution curve). In addition, the frequency range $f \in [40, 80]$ Hz is also acceptable as their average travelling times are 61.2, 47.8, 37.2, 46.6 and 49.6 seconds, respectively. The secondary experiment examining the capsule's dynamic behaviours will focus on this range.

B. Preliminary duty cycle

To compare the travelling time under different D, we considered f from 10 Hz to 100 Hz in each group of D. As can be seen from Fig. 8(c), the experiments show that the best working D is 30% and 50%, with the shortest average travelling time of 67.4 s and 67.3 s, respectively. As these two values are very close, we then compare the behaviour from the normal distribution of the experiments under the same D group, and it appears that 30% is slightly more stable than 50%. During the experiment, as the impact becomes rather a constant applied force on the capsule when D is larger, the capsule is more likely to flip over when crossing the fold and stuck at the bottom of the fold. To summarise, it is determined that $D = 30\%$ will be the optimum duty cycle to conduct the secondary experiment.

C. Total maneuver time

According to the preliminary results, the optimum duty cycle and frequency are $D = 30\%$ and $f \in [40, 80]$ Hz, respectively. We then conducted a second round experiment with five frequencies in 40, 50, 60, 70 and 80 Hz, all of which were under 30% duty cycle. Each group of the experiments was performed five times to maintain its consistency, where $f \in [40, 60]$ Hz presented a more stable movement than $f \in [70, 80]$ Hz revealed by the maneuver time differences. The trajectories for these five groups of experiments are plotted in Fig. 9, where the travelling time at each section is presented. Based on the experimental results, the capsule's maximum speed of 54 mm/s was found at $f = 60$ Hz.

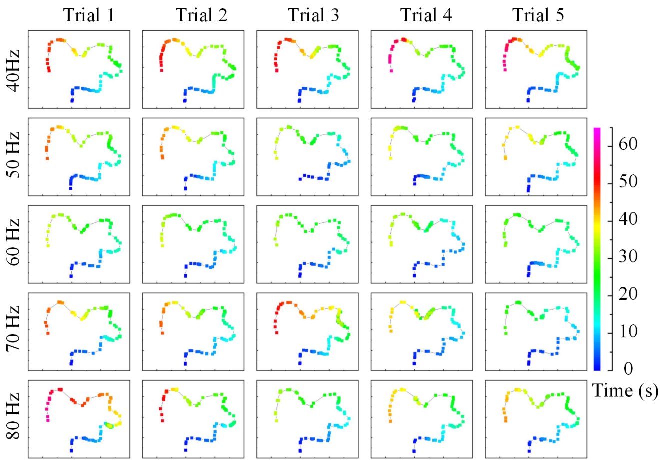

Fig. 9. Trace plots of the second round experiment videos, all of which were under D=30%, and each frequency was repeated by five times to show its consistency. Colour bar on the right panel indicates the travelling time.

D. Travelling time at specific turns

During the experiment, an interesting observation is that the capsule under different excitation frequencies responses to the sections of simulator differently. This observation can help to understand how to control the capsule efficiently by reducing its side movements. As 12 sections of the simulator were considered as shown in Fig. 7, it was found that under low control frequencies $f \in [10, 30]$ Hz, the capsule was more likely to face difficulties in crossing certain turns and folds, while with a high frequency $f \in [80, 100]$ Hz these turns were smoothly passed; and vice versa. Table III lists the passing times of the capsule on Sections ⑦ and ⑨ of the simulator under different excitation frequencies with $D = 30\%$ and 40% from the preliminary experiments. For both duty cycles, a low frequency is preferred than a high one for Section ⑦, while a high frequency is preferred than a low one for Section ⑨. As can be seen from the table, the travelling times are dramatically different under $D = 40\%$ at Section ⑨. Overall, the capsule can pass some sections smoothly, such as Sections ③, ④ and ⑫, while on ⑦, ⑨ and ⑩, the movements tend to be unstable and time-consuming.

For the entire experiment, it was found that with the lowest success rate in the capsule's first attempt to pass the turn occurred at the rectosigmoid junction ① and the sigmoid-descending junction ⑤. The first one is a relatively straight path with a slightly higher haustral fold compared to the others, which results in a greater requirement to lift the capsule against its gravity and barely no reaction force from the corner of colon wall to help the capsule climb through at any frequencies. The second one is a fold followed by a sharp turn, so the capsule needs force with a tricky angle to get through, especially with the frequencies under 30 Hz. For the frequencies above 30 Hz, this section can be passed smoothly. This finding indicates that the optimal control parameters may not be constant during navigation, especially when encountering sharp turns inside the intestine. During the procedure, optimum f and D can be adjusted by the operator in real time according to various intestinal environments.

TABLE III

PASSING TIMES (IN SECONDS) AT SPECIFIC TURNS.

D	f (Hz)	10	20	30	80	90	100
30%	⑦	3.5	7	4	5	6	16.5
	⑨	33	24	25.5	3	1.5	2
40%	⑦	5.5	2	4.5	15	4	5
	⑨	77	49	14	4	2.5	4

E. Ex vivo experiments

Ex vivo experiments were carried out by using the experimental setup described in Sec. II-E. A demonstration of success of a completed *ex vivo* journey is presented in Fig. 10, where the capsule prototype was able to turn itself over and travel back from the cecum to the rectum controlled by the electromagnetic coil panel.

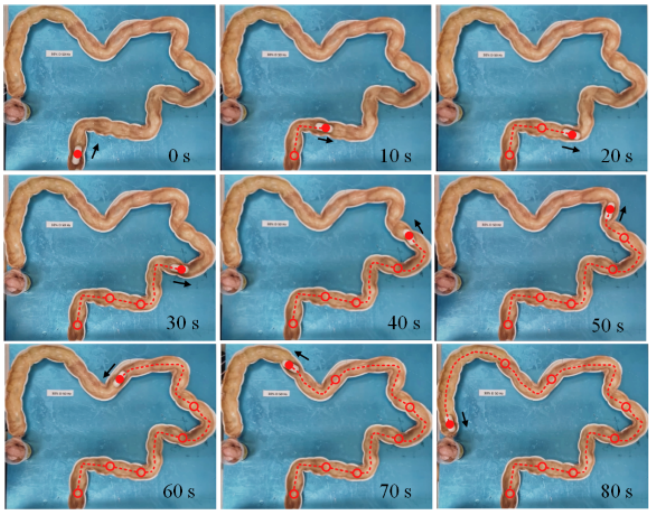

Fig. 10. Capsule's *ex vivo* trajectory by using porcine intestine on the rigid simulator under f=50 Hz and D=30% with an average speed of 20 mm/s.

Ten experimental attempts were carried out under $D = 30\%$ and $f \in [10, 100]$ Hz. Table IV presents the average travelling speeds. The trend is similar to the bare-surface first round experiment, where a low frequency led to a low progression speed, and the best frequency range is around 50-60 Hz. However, with $f = 100$ Hz it can also achieve a high progression speed, which is different from the bare-surface experiments. The difference between the *ex vivo* and bare-surface experiments is the intestine tissue, which may cause the contact surface of the capsule prototype viscous and slippery. In this scenario, when $f = 100$ Hz, it performed stable and the capsule was able to cross the haustral folds at a fast speed, while addressing some difficulties encountered in the bare-surface experiment due to the less powerful capsule.

Another *ex vivo* experiment shown in Fig. 11 was carried out on a soft simulator (fabricated with 25 pores per inch sponge foam) with a similar shape to the rigid one covered

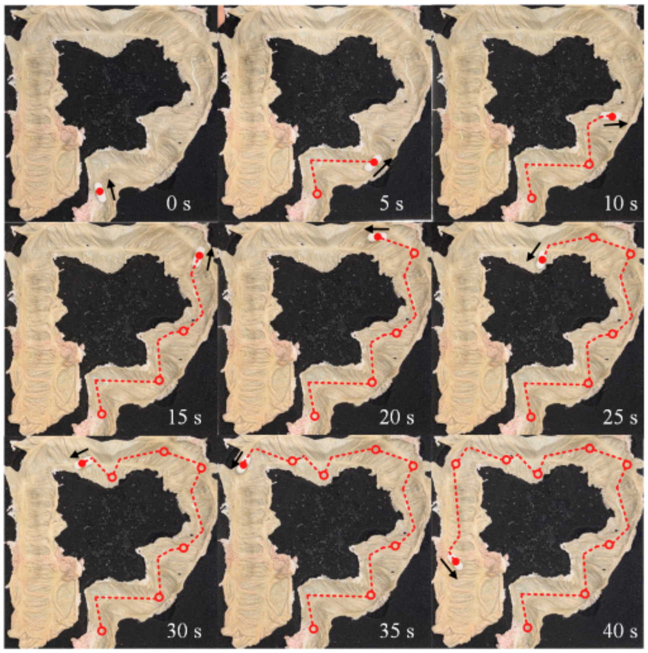

Fig. 11. Capsule's *ex vivo* trajectory by using porcine intestine on the soft simulator under f=60 Hz and D=30% with an average speed of 40 mm/s.

TABLE IV

AVERAGE SPEEDS OF *EX VIVO* TESTS UNDER $D = 30\%$.

f (Hz)	10	20	30	40	50
Speed (mm/s)	7.1	12.6	10.9	16.8	20
f (Hz)	60	70	80	90	100
Speed (mm/s)	18.2	15	15	13.4	19.8

by the fresh porcine large intestine tissue acquired from a local abattoir. The experiment was repeated four times with the total travelling time of 48, 44, 42 and 40 seconds, respectively, under f=60 Hz and D=30%.

IV. CONCLUSIONS

In this paper, we aimed to equip a vibro-impact propulsion module into a colon-fitted sized untethered capsule for large intestine examination, demonstrating the concept of the vibro-impact driving method and proving its maneuverability in *ex vivo* tests. We optimised the configuration of a hand-held coil panel in order to obtain the best driving force to maneuver the capsule prototype. The optimum progression speed of the capsule inside an intestinal environment with various excitation frequencies and duty cycles was also investigated experimentally. However, the drawback is that the hand-held method requires the operator to be conscious about the capsule's position and its surrounding environment. During our experiments, the internal environment of the large intestine was supposed to be known. From this point of view, lacks of localisation and on-board visualisation systems become the main limitations of our current prototype. As a future work, an on-board camera and a real-time localisation system (e.g., [26]) will be integrated. By combining the information of capsule's position and orientation, desired coil motion can be calculated from the proposed numerical solution to guide the operator for an efficient examination.

REFERENCES

[1] J. Martin, et al., "Enabling the future of colonoscopy with intelligent and autonomous magnetic manipulation," *Nat. Mach. Intell.*, vol. 2, pp. 595–606, 2020.

[2] E. Mooiweer, et al., "Incidence of interval colorectal cancer among inflammatory bowel disease patients undergoing regular colonoscopic surveillance," *Clin. Gastroenterol. Hepatol.*, vol. 13, pp. 1656–61, 2015.

[3] O. Onaizah, et al., "Guidelines for Robotic Flexible Endoscopy at the Time of COVID-19," *Clin. Gastroenterol. Hepatol.*, vol. 8, 2021.

[4] F. Vuik, et al., "Colon capsule endoscopy in colorectal cancer screening: a systematic review," *Endoscopy*, vol. 53, pp. 815–24, 2021.

[5] J. Westerhof, J.J. Koornstra and R.K. Weersma, "Capsule endoscopy: a review from the clinician's perspectives," *Minerva Gastroenterol Dietol*, vol. 54, pp. 189–207, 2008.

[6] C. Poon, et al., "Design of wormlike automated robotic endoscope: dynamic interaction between endoscopic balloon and surrounding tissues," *Surg. Endosc.*, vol. 30, pp. 772–8, 2015.

[7] D. Lee, S. Joe, H. Kang, T. An and B. Kim, "A reel mechanism-based robotic colonoscope with high safety and maneuverability," *Surg. Endosc.*, vol. 33, pp. 322–32, 2018.

[8] M. Chauhan, J. Chandler, A. Jha, V. Subramaniam, K. Obstein, P. Valdastri, "An origami-based soft robotic actuator for upper gastrointestinal endoscopic applications," *Front. Robot. AI*, vol. 8, 664720, 2021.

[9] W. Xin F. Pan Y. Li P. Chiu, Z. Li, "Design and modeling of a biomimetic gastropod-like soft robot with wet adhesive locomotion," *IEEE Int. Conf. Robot. Autom.*, pp. 11997–2003, 2021.

[10] N. Shamsudhin, et al., "Magnetically guided capsule endoscopy," *Med. Phys.*, vol. 44, pp. e91–e111, 2017.

[11] A. Mahoney, J. Abbott, "Five-degree-of-freedom manipulation of an untethered magnetic device in fluid using a single permanent magnet with application in stomach capsule endoscopy," *Int. J. Rob. Res.*, vol. 35(1–3), pp. 129—147, 2016.

[12] P. Dupont, et al., "A decade retrospective of medical robotics research from 2010 to 2020," *Sci. Robot.*, vol. 6, eabi8017, 2021.

[13] Y. Xu, K. Li, Z. Zhao, M. Meng, "Adaptive simultaneous magnetic actuation and localization for WCE in a tubular environment," *IEEE Trans. Robot.*, pp. 1–10, 2022.

[14] X. Jiang, J. Pan, Z. Li, Z. Liao, "Standardized examination procedure of magnetically controlled capsule endoscopy," *VideoGIE*, vol. 4, pp. 239–43, 2019.

[15] D. Son, H. Gilbert, M. Sitti, "Magnetically actuated soft capsule endoscope for fine-needle biopsy," *Soft Robot.*, vol. 7, pp. 10–21, 2020.

[16] G. Pittiglio, et al., "Software for enhanced video capsule endoscopy: challenges for essential progress," *Nat. Rev. Gastro. Hepat.*, vol. 4, pp. 1224–31, 2019.

[17] F. Munoz, et al., "Analysis of magnetic interaction in remotely controlled magnetic devices and its application to a capsule robot for drug delivery," *IEEE-ASME T. Mech.*, vol. 23, pp. 298–310, 2018.

[18] L. Zheng, S. Guo, Z. Wang, T. Tamiya, "A multi-functional module-based capsule robot," *IEEE Sens. J.*, vol. 21, pp. 12057–67, 2021.

[19] Y. Liu, M. Wiercigroch, E. Pavlovskaia and H. Yu, "Modeling of a vibro-impact capsule system," *Int. J. Mech. Sci.*, vol. 66, pp. 2–11, 2013.

[20] Y. Yan, Y. Liu, L. Manfredi and S. Prasad, "Modelling of a vibro-impact self-propelled capsule in the small intestine," *Nonlinear Dyn.*, vol. 96, pp. 123–144, 2019.

[21] J. Zhang, Y. Liu, D. Zhu, S. Prasad and C. Liu, "Simulation and experimental studies of a vibro-impact capsule system driven by an external magnetic field," *Nonlinear Dyn.*, vol. 109, pp. 1501–16, 2022.

[22] M. Sfakiotakis, N. Pateromichelakis, D. Tsakiris, "Vibration-induced frictional reduction in miniature intracorporeal robots," *IEEE Trans. Robot.*, vol. 206, pp. 1210–1221, 2014.

[23] J. Barducci, et al., "Fundamentals of the gut for capsule engineers," *Prog. Biomed. Eng.*, vol. 2, 042002, 2020.

[24] H. A. Wheeler, "Simple inductance formulas for radio coils," *PIRE*, vol. 16, no. 10, pp. 1398–400, 1928.

[25] G. Giovannetti, "Comparison between circular and square loops for low-frequency magnetic resonance applications: theoretical performance estimation," *Concepts Magn. Reson. Part B*, vol. 46B, no. 3, pp. 146–55, 2016.

[26] D. Son, S. Yim, M. Sitti, "A 5-D localization method for a magnetically manipulated untethered robot using a 2-D array of hall-effect sensors," *IEEE-ASME T. Mech.*, vol. 21, pp. 708–16, 2016.